

Dynamics of particle sedimentation in viscoelastic fluids: A numerical study on particle chain in two-dimensional narrow channel

Tsorng-Whay Pan*

Department of Mathematics, University of Houston, Houston, Texas 77204, USA

Roland Glowinski

Department of Mathematics, University of Houston, Houston, Texas 77204, USA

Department of Mathematics, Hong Kong Baptist University, Hong Kong

Abstract

In this article we present a numerical method for simulating the sedimentation of circular particles in two-dimensional channel filled with a viscoelastic fluid of FENE-CR type, which is generalized from a domain/distributed Lagrange multiplier method with a factorization approach for Oldroyd-B fluids developed in [J. Non-Newtonian Fluid Mech. 156 (2009) 95]. Numerical results suggest that the polymer extension limit L for the FENE-CR fluid has no effect on the final formation of vertical chain for the cases of two disks and three disks in two-dimensional narrow channel, at least for the values of L considered in this article; but the intermediate dynamics of particle interaction before having a vertical chain can be different for the smaller values of L when increasing the relaxation time. For the cases of six particles sedimenting in FENE-CR type viscoelastic fluid, the formation of chain of 4 to 6 disks does depend on the polymer extension limit L . For the smaller values of L , FENE-CR type viscoelastic fluid can not bring them together like the case of these particles settling in a vertical chain formation in Oldroyd-B fluid; but two separated chains of three disks are formed. Similar results for the case of ten disks are also obtained. The numerical results of several more particle cases suggest that for smaller values of L , the length of the vertical chain is shorter and the size of cluster is smaller.

Keywords: Oldroyd-B fluid, FENE-CR model, Positive definiteness, Fictitious domain, Particulate flow

1 Introduction

The motion of particles in non-Newtonian fluids is not only of fundamental theoretical interest, but is also of importance in many applications to industrial processes involving particle-laden materials (see, e.g., [1] and [2]). For example, during the hydraulic fracturing operation used in oil and gas wells, suspensions of solid particles in polymeric solutions are pumped into hydraulically-induced fractures. The particles must prop these channels open to enhance the rate of oil recovery [3]. During the shut-in stage, proppant settling is pronounced when the fluid pressure decreases due to the end of hydraulic fracturing process. The study of particle chain during settling in vertical channel can help us to understand the mechanism of proppant agglomeration in narrow fracture zones [4].

Although numerical methods for simulating particulate flows in Newtonian fluids have been very successful, numerically simulating particulate flows in viscoelastic fluids is much more complicated and challenging. One of the difficulties (e.g., see [5], [6]) for simulating viscoelastic flows is the breakdown of the numerical

*pan@math.uh.edu

methods. It has been widely believed that the lack of positive definiteness preserving property of the conformation tensor at the discrete level during the *entire time integration* is one of the reasons for the breakdown. To preserve the positive definiteness property of the conformation tensor, several methodologies have been proposed recently, as in [7], [8], [9] and [10]. Lozinski and Owens [10] factored the conformation tensor to get $\sigma = AA^T$ and then they wrote down the equations for A approximately at the discrete level. Hence, the positive definiteness of the conformation tensor is forced with such an approach. The methodologies developed in [10] have been applied in [11] together with the FD/DLM method through operator splitting techniques for simulating particulate flows in Oldroyd-B fluid. We have generalized these computational methodologies to viscoelastic fluids of the FENE-CR type, which is a more “realistic” model when compared with the Oldroyd-B model as advocated in [12]. To study the effect of the polymer extension limit L on the particle chain formation while settling, we have considered the cases of two, three and six disks settling in viscoelastic fluid is previously considered in [11] since vertical chains are known to be formed for these cases. In this article, we have compared the particle sedimenting in a vertical two-dimensional channel filled with viscoelastic fluid of either Oldroyd-B or FENE-CR types to find out the effect of the extension limit of the immersed polymer coils on the chaining. The computational results of disks settling in Oldroyd-B fluid are obtained by the numerical method developed in [11]. For the cases of two disks and three disks in two-dimensional narrow channel, numerical results suggest that the polymer extension limit L for the FENE-CR fluid has no effect on the final formation of vertical particle chain, at least for the values of L considered in this article; but the intermediate particle dynamics can be different for the smaller values of L when increasing the value of the relaxation time. For six particles sedimenting in FENE-CR type viscoelastic fluid, the formation of chain of 4 to 6 disks does depend on the polymer extension limit L . For the smaller values of L , FENE-CR type viscoelastic fluid can not bring them together like the case of these particles settling in a vertical chain formation in Oldroyd-B fluid; but instead two separated chains of three disks are formed. Similar results for the case of ten disks are also obtained. The numerical results of several more particle cases suggest that for smaller values of L , the length of the vertical chain is shorter and the size of cluster is smaller. The article is organized as follows. In Section 2, we present a FD/DLM formulation for particulate flows in an FENE-CR fluid and the associated the operator splitting technique, the space and time discretization of the FD/DLM formulation, how we apply the Lozinski and Owens method to get the equivalent equations for the conformation tensor. In Section 3, numerical results for the cases of sedimentation of two, three, and six particles and their chaining under the effect of the the polymer extension are discussed.

2 Mathematical Formulations and numerical methods

2.1 Governing equations and its FD/DLM Formulation

Following the work developed in [11], we will first address in the following the models and computational methodologies combined with the Lozinski and Owens’ factorization approach. Let Ω be a bounded two-dimensional (2D) domain and let Γ be the boundary of Ω . We suppose that Ω is filled with a viscoelastic fluid of either Oldroyd-B or FENE-CR type of density ρ_f and that it contains N moving rigid particles of density ρ_s (see Figure 1). Let $B(t) = \cup_{i=1}^N B_i(t)$ where $B_i(t)$ is the i th rigid particle in the fluid for $i = 1, \dots, N$. We denote by $\partial B_i(t)$ the boundary of $B_i(t)$ for $i = 1, \dots, N$. For some $T > 0$, the governing equations for

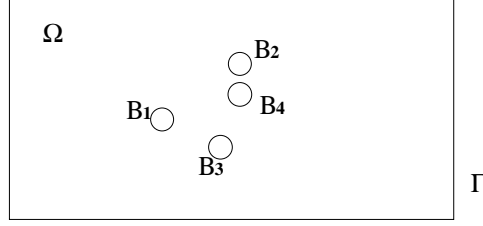


Figure 1: An example of a two-dimensional flow region with four circular particles.

the fluid-particle system are

$$\rho_f \left(\frac{\partial \mathbf{u}}{\partial t} + (\mathbf{u} \cdot \nabla) \mathbf{u} \right) = \rho_f \mathbf{g} - \nabla p + 2\mu \nabla \cdot \mathbf{D}(\mathbf{u}) + \nabla \cdot \boldsymbol{\sigma}^p \quad \text{in } \Omega \setminus \overline{B(t)}, \quad t \in (0, T), \quad (1)$$

$$\nabla \cdot \mathbf{u} = 0 \quad \text{in } \Omega \setminus \overline{B(t)}, \quad t \in (0, T), \quad (2)$$

$$\mathbf{u}(\mathbf{x}, 0) = \mathbf{u}_0(\mathbf{x}), \quad \forall \mathbf{x} \in \Omega \setminus \overline{B(0)}, \quad \text{with } \nabla \cdot \mathbf{u}_0 = 0, \quad (3)$$

$$\mathbf{u} = \mathbf{g}_0 \quad \text{on } \Gamma \times (0, T), \quad \text{with } \int_{\Gamma} \mathbf{g}_0 \cdot \mathbf{n} \, d\Gamma = 0, \quad (4)$$

$$\mathbf{u} = \mathbf{V}_{p,i} + \omega_i \times \overrightarrow{\mathbf{G}_i \mathbf{x}}, \quad \forall \mathbf{x} \in \partial B_i(t), \quad i = 1, \dots, N, \quad (5)$$

$$\frac{\partial \mathbf{C}}{\partial t} + (\mathbf{u} \cdot \nabla) \mathbf{C} - (\nabla \mathbf{u}) \mathbf{C} - \mathbf{C} (\nabla \mathbf{u})^t = -\frac{f(\mathbf{C})}{\lambda_1} (\mathbf{C} - \mathbf{I}) \quad \text{in } \Omega \setminus \overline{B(t)}, \quad t \in (0, T), \quad (6)$$

$$\mathbf{C}(\mathbf{x}, 0) = \mathbf{C}_0(\mathbf{x}), \quad \mathbf{x} \in \Omega \setminus \overline{B(0)}, \quad (7)$$

$$\mathbf{C} = \mathbf{C}_L, \quad \text{on } \Gamma^-, \quad (8)$$

where \mathbf{u} is the flow velocity, p is the pressure, \mathbf{g} is the gravity, $\mu = \eta_1 \lambda_2 / \lambda_1$ is the solvent viscosity of the fluid, $\eta = \eta_1 - \mu$ is the elastic viscosity of the fluid, η_1 is the fluid viscosity, λ_1 is the relaxation time of the fluid, λ_2 is the retardation time of the fluid, \mathbf{n} is the outer normal unit vector at Γ , Γ^- is the upstream portion of Γ . The polymeric stress tensor $\boldsymbol{\sigma}^p$ in (1) is given by $\boldsymbol{\sigma}^p = \frac{\eta}{\lambda_1} f(\mathbf{C})(\mathbf{C} - \mathbf{I})$, where the conformation tensor \mathbf{C} is symmetric and positive definite (see [13]) and \mathbf{I} is the identity matrix. Setting f equal to unity corresponds to the Oldroyd-B model while

$$f(\mathbf{C}) = \frac{L^2}{L^2 - \text{tr}(\mathbf{C})} \quad (9)$$

corresponds to the FENE-CR model [14], where $\text{tr}(\mathbf{C})$ is the trace of the conformation tensor \mathbf{C} and L is the maximum extension of the immersed polymer coils and referred to as the extensibility of the immersed polymer coils. The Oldroyd-B model then is a special case associated with infinite extensibility.

In (5), the no-slip condition holds on the boundary of the i th particle, $\mathbf{V}_{p,i}$ is the translation velocity, ω_i is the angular velocity and \mathbf{G}_i is the center of mass and $\omega_i \times \overrightarrow{\mathbf{G}_i \mathbf{x}} = (-\omega_i(x_2 - G_{i,2}), \omega_i(x_1 - G_{i,1}))$ (for 2D cases considered in this article). The motion of the particles is modeled by Newton's laws:

$$M_{p,i} \frac{d\mathbf{V}_{p,i}}{dt} = M_{p,i} \mathbf{g} + \mathbf{F}_i + \mathbf{F}_i^r, \quad (10)$$

$$I_{p,i} \frac{d\omega_i}{dt} = F_i^t, \quad (11)$$

$$\frac{d\mathbf{G}_i}{dt} = \mathbf{V}_{p,i}, \quad (12)$$

$$\mathbf{G}_i(0) = \mathbf{G}_i^0, \quad \mathbf{V}_{p,i}(0) = \mathbf{V}_{p,i}^0, \quad \omega_i(0) = \omega_i^0, \quad (13)$$

for $i = 1, \dots, N$, where in (10)-(13), $M_{p,i}$ and $I_{p,i}$ are the mass and the inertia of the i th particle, respectively, \mathbf{F}_i^r is a short range repulsion force imposed on the i th particle by other particles and the wall to prevent particle/particle and particle/wall penetration (see [15] for details), and \mathbf{F}_i and F_i^t denote the hydrodynamic force and the associated torque imposed on the i th particle by the fluid, respectively.

To avoid the frequent remeshing and the difficulty of the mesh generation for a time-varying domain in which the rigid particles can be very close to each other, especially for three dimensional particulate flow, we have extended the governing equations to the entire domain Ω (a fictitious domain). For a fictitious-domain-based variational formulation of the governing equations of the particulate flow, we consider only one rigid particle $B(t)$ (a disk in 2D) in the fluid domain without losing generality. Let us define first the following functional spaces

$$\begin{aligned}\mathbf{V}_{\mathbf{g}_0(t)} &= \{ \mathbf{v} \mid \mathbf{v} \in (H^1(\Omega))^2, \mathbf{v} = \mathbf{g}_0(t) \text{ on } \Gamma \}, \\ L_0^2(\Omega) &= \{ q \mid q \in L^2(\Omega), \int_{\Omega} q \, d\mathbf{x} = 0 \}, \\ \mathbf{V}_{\mathbf{C}_L(t)} &= \{ \mathbf{C} \mid \mathbf{C} \in (H^1(\Omega))^{2 \times 2}, \mathbf{C} = \mathbf{C}_L(t) \text{ on } \Gamma^- \}, \\ \mathbf{V}_{\mathbf{C}_0} &= \{ \mathbf{C} \mid \mathbf{C} \in (H^1(\Omega))^{2 \times 2}, \mathbf{C} = 0 \text{ on } \Gamma^- \}, \\ \Lambda(t) &= H^1(B(t))^2.\end{aligned}$$

Following the methodologies developed in [15, 16], a fictitious domain formulation of the governing equations (1)-(13) reads as follows:

For a.e. $t > 0$, find $\mathbf{u}(t) \in \mathbf{V}_{\mathbf{g}_0(t)}$, $p(t) \in L_0^2(\Omega)$, $\mathbf{C}(t) \in \mathbf{V}_{\mathbf{C}_L(t)}$, $\mathbf{V}(t) \in \mathbb{R}^2$, $\mathbf{G}(t) \in \mathbb{R}^2$, $\omega(t) \in \mathbb{R}$, $\boldsymbol{\lambda}(t) \in \Lambda(t)$ such that

$$\begin{cases} \rho_f \int_{\Omega} \left[\frac{\partial \mathbf{u}}{\partial t} + (\mathbf{u} \cdot \nabla) \mathbf{u} \right] \cdot \mathbf{v} \, d\mathbf{x} + 2\mu \int_{\Omega} \mathbf{D}(\mathbf{u}) : \mathbf{D}(\mathbf{v}) \, d\mathbf{x} - \int_{\Omega} p \nabla \cdot \mathbf{v} \, d\mathbf{x} \\ - \int_{\Omega} \mathbf{v} \cdot (\nabla \cdot \boldsymbol{\sigma}^p) \, d\mathbf{x} + (1 - \rho_f/\rho_s) \{ M_p \frac{d\mathbf{V}}{dt} \cdot \mathbf{Y} + I_p \frac{d\omega}{dt} \cdot \theta \} \\ - \langle \boldsymbol{\lambda}, \mathbf{v} - \mathbf{Y} - \theta \times \overrightarrow{\mathbf{G}\mathbf{x}} \rangle_{B(t)} - \mathbf{F}^r \cdot \mathbf{Y} \\ = \rho_f \int_{\Omega} \mathbf{g} \cdot \mathbf{v} \, d\mathbf{x} + (1 - \rho_f/\rho_s) M_p \mathbf{g} \cdot \mathbf{Y}, \\ \forall \{ \mathbf{v}, \mathbf{Y}, \theta \} \in (H_0^1(\Omega))^2 \times \mathbb{R}^2 \times \mathbb{R}, \end{cases} \quad (14)$$

$$\int_{\Omega} q \nabla \cdot \mathbf{u}(t) \, d\mathbf{x} = 0, \forall q \in L^2(\Omega), \quad (15)$$

$$\langle \boldsymbol{\mu}, \mathbf{u}(\mathbf{x}, t) - \mathbf{V}(t) - \omega(t) \times \overrightarrow{\mathbf{G}(t)\mathbf{x}} \rangle_{B(t)} = 0, \quad \forall \boldsymbol{\mu} \in \Lambda(t), \quad (16)$$

$$\int_{\Omega} \left(\frac{\partial \mathbf{C}}{\partial t} + (\mathbf{u} \cdot \nabla) \mathbf{C} - (\nabla \mathbf{u}) \mathbf{C} - \mathbf{C} (\nabla \mathbf{u})^t \right) : \mathbf{s} \, d\mathbf{x} \quad (17)$$

$$= - \int_{\Omega} \frac{f(\mathbf{C})}{\lambda_1} (\mathbf{C} - \mathbf{I}) : \mathbf{s} \, d\mathbf{x}, \forall \mathbf{s} \in \mathbf{V}_{\mathbf{C}_0}, \text{ with } \mathbf{C} = \mathbf{I} \text{ in } B(t),$$

$$\frac{d\mathbf{G}}{dt} = \mathbf{V}, \quad (18)$$

$$\mathbf{C}(\mathbf{x}, 0) = \mathbf{C}_0(\mathbf{x}), \forall \mathbf{x} \in \Omega, \text{ with } \mathbf{C}_0 = \mathbf{I} \text{ in } B(0), \quad (19)$$

$$\mathbf{G}(0) = \mathbf{G}_0, \mathbf{V}(0) = \mathbf{V}_0, \omega(0) = \omega_0, B(0) = B_0, \quad (20)$$

$$\mathbf{u}(\mathbf{x}, 0) = \begin{cases} \mathbf{u}_0(\mathbf{x}), \forall \mathbf{x} \in \Omega \setminus \overline{B_0}, \\ \mathbf{V}_0 + \omega_0 \times \overrightarrow{\mathbf{G}_0 \mathbf{x}}, \forall \mathbf{x} \in \overline{B_0}. \end{cases} \quad (21)$$

In (14) the *Lagrange multiplier* $\boldsymbol{\lambda}$ defined over B can be viewed as an extra body force maintaining the rigid body motion inside B . The conformation tensor \mathbf{C} inside the rigid particle is extended as the identity tensor

\mathbf{I} as in (17) since the polymeric stress tensor is zero inside the rigid particle. In equation (14), since \mathbf{u} is divergence free and satisfies the Dirichlet boundary conditions on Γ , we have $2 \int_{\Omega} \mathbf{D}(\mathbf{u}) : \mathbf{D}(\mathbf{v}) d\mathbf{x} = \int_{\Omega} \nabla \mathbf{u} : \nabla \mathbf{v} d\mathbf{x}$, $\forall \mathbf{v} \in (H_0^1(\Omega))^2$. This is a substantial simplification from the computational point of view, which is another advantage of the fictitious domain approach. With this simplification, we can use, as shown in the following section, fast solvers for the elliptic problems in order to speed up computations. Also the gravity term \mathbf{g} in (14) can be absorbed in the pressure term.

2.2 Finite Element Approximation

In order to solve problem (14)-(21) numerically, we shall discretize the fictitious domain Ω using an uniform finite element mesh \mathcal{T}_h for the velocity and conformation tensor, where h is the mesh size, and a twice coarser uniform mesh \mathcal{T}_{2h} for the pressure. The following finite dimensional spaces are defined for approximating $\mathbf{V}_{\mathbf{g}_0(t)}$, $(H_0^1(\Omega))^2$, $L^2(\Omega)$, $L_0^2(\Omega)$, $\mathbf{V}_{\mathbf{C}_L(t)}$, $\mathbf{V}_{\mathbf{C}_0}$, respectively,

$$\begin{aligned} \mathbf{V}_{\mathbf{g}_{0h}(t)} &= \{ \mathbf{v}_h \mid \mathbf{v}_h \in (C^0(\overline{\Omega}))^2, \mathbf{v}_h|_E \in (P_1)^2, \forall E \in \mathcal{T}_h, \mathbf{v}_h|_{\Gamma} = \mathbf{g}_{0h}(t) \}, \\ \mathbf{V}_{0h} &= \{ \mathbf{v}_h \mid \mathbf{v}_h \in (C^0(\overline{\Omega}))^2, \mathbf{v}_h|_E \in (P_1)^2, \forall E \in \mathcal{T}_h, \mathbf{v}_h|_{\Gamma} = 0 \}, \\ L_h^2 &= \{ q_h \mid q_h \in C^0(\overline{\Omega}), q_h|_E \in P_1, \forall E \in \mathcal{T}_{2h} \}, \\ L_{0h}^2 &= \{ q_h \mid q_h \in L_h^2, \int_{\Omega} q_h d\mathbf{x} = 0 \}, \\ \mathbf{V}_{\mathbf{C}_{Lh}(t)} &= \{ s_h \mid s_h \in (C^0(\overline{\Omega}))^{2 \times 2}, s_h|_E \in (P_1)^{2 \times 2}, \forall E \in \mathcal{T}_h, s_h|_{\Gamma_h^-} = \mathbf{C}_{Lh}(t) \}, \\ \mathbf{V}_{\mathbf{C}_{0h}} &= \{ s_h \mid s_h \in (C^0(\overline{\Omega}))^{2 \times 2}, s_h|_E \in (P_1)^{2 \times 2}, \forall E \in \mathcal{T}_h, s_h|_{\Gamma_h^-} = 0 \} \end{aligned}$$

where P_1 is the space of the polynomials in two variables of degree ≤ 1 , $\mathbf{g}_{0h}(t)$ is an approximation of \mathbf{g}_0 satisfying $\int_{\Gamma} \mathbf{g}_{0h}(t) \cdot \mathbf{n} d\Gamma = 0$, and $\Gamma_h^- = \{ \mathbf{x} \mid \mathbf{x} \in \Gamma, \mathbf{g}_{0h}(\mathbf{x}, t) \cdot \mathbf{n}(\mathbf{x}) < 0 \}$. The discrete Lagrange multiplier space $\Lambda_h(t)$ is defined as follows: let $\{\mathbf{x}_i\}_{i=1}^K$ be a set of points from $\overline{B(t)}$ that covers $\overline{B(t)}$ evenly, and then we define

$$\Lambda_h(t) = \{ \boldsymbol{\mu} \mid \boldsymbol{\mu} = \sum_{j=1}^K \boldsymbol{\mu}_j \delta(\mathbf{x} - \mathbf{x}_j), \boldsymbol{\mu}_j \in \mathbb{R}^2, \forall j = 1, \dots, K \}, \quad (22)$$

where $\mathbf{x} \rightarrow \delta(\mathbf{x} - \mathbf{x}_j)$ is the Dirac measure at \mathbf{x}_j . Then instead of the scalar product of $(H^1(B_h(t)))^2$, we shall use $\langle \boldsymbol{\mu}, \mathbf{v} \rangle_{B_h(t)}$ defined by

$$\langle \boldsymbol{\mu}, \mathbf{v} \rangle_{B_h(t)} = \sum_{j=1}^K \boldsymbol{\mu}_j \cdot \mathbf{v}(\mathbf{x}_j), \forall \boldsymbol{\mu} \in \Lambda_h(t), \mathbf{v} \in \mathbf{V}_{\mathbf{g}_{0h}(t)} \text{ or } \mathbf{V}_{0h}. \quad (23)$$

Using the above scalar product implies that the rigid body motion of $B(t)$ is forced via a *collocation method* [15].

Then a discrete analogue of the problem (14)-(21) can be obtained with the above finite dimensional spaces.

2.3 An Operator Splitting Scheme

Consider the following initial value problem:

$$\frac{d\phi}{dt} + A(\phi) = 0 \text{ on } (0, T), \quad \phi(0) = \phi_0 \quad (24)$$

with $0 < T < +\infty$. We suppose that operator A has a decomposition such as $A = \sum_{j=1}^J A_j$ with $J \geq 2$. Let $\tau(> 0)$ be a time-discretization step, we denote $n\tau$ by t^n . With ϕ^n denoting an approximation of $\phi(t^n)$, the **Lie scheme** [17] reads as follows:

For $n \geq 0$, assuming that ϕ^n is known (with $\phi^0 = \phi_0$), compute ϕ^{n+1} via

$$\begin{cases} \frac{d\phi}{dt} + A_j(\phi) = 0 & \text{on } (t^n, t^{n+1}), \\ \phi(t^n) = \phi^{n+(j-1)/J}; \phi^{n+j/J} = \phi(t^{n+1}), \end{cases} \quad (25)$$

for $j = 1, \dots, J$. The Lie's scheme is first order accurate, but its low order of accuracy is compensated by its simplicity, making it (relatively) easy to implement, and by its robustness. Some classical operator splitting techniques with application to the Navier-Stokes equations have been discussed in [18] in details.

The Lie's operator splitting scheme allows us to decouple the following difficulties:

- (1). The incompressibility condition, and the related unknown pressure;
- (2). The advection terms;
- (3). The rigid-body motion in $B_h(t)$, and the related DLM λ_h .

The constitutive equation satisfied by the conformation tensor \mathbf{C} is split with $J = 3$ for now to show how the factorization approach works out. Suppose that \mathbf{C}^n and \mathbf{u} are known, we compute

$$\begin{cases} \frac{d\mathbf{C}}{dt} + (\mathbf{u} \cdot \nabla)\mathbf{C} = 0 & \text{on } (t^n, t^{n+1}), \\ \mathbf{C}(t^n) = \mathbf{C}^n; \mathbf{C}^{n+1/3} = \mathbf{C}(t^{n+1}), \end{cases} \quad (26)$$

$$\begin{cases} \frac{d\mathbf{C}}{dt} - (\nabla\mathbf{u})\mathbf{C} - \mathbf{C}(\nabla\mathbf{u})^t + \frac{f(\mathbf{C}^{n+1/3})}{\lambda_1}\mathbf{C} = 0 & \text{on } (t^n, t^{n+1}), \\ \mathbf{C}(t^n) = \mathbf{C}^{n+1/3}; \mathbf{C}^{n+2/3} = \mathbf{C}(t^{n+1}), \end{cases} \quad (27)$$

$$\begin{cases} \frac{d\mathbf{C}}{dt} = \frac{f(\mathbf{C}^{n+2/3})}{\lambda_1}\mathbf{I} & \text{on } (t^n, t^{n+1}), \\ \mathbf{C}(t^n) = \mathbf{C}^{n+2/3}; \mathbf{C}^{n+1} = \mathbf{C}(t^{n+1}). \end{cases} \quad (28)$$

We have derived the following two equivalent equations based on the factorization approach with $s = f(\mathbf{C}^{n+1/3})$ for equations (26) and (27):

Lemma 2.1. *For a matrix A and $\mathbf{C} = AA^t$, given the velocity \mathbf{u} , $\lambda_1(> 0)$ and a constant s ,*

(a). *if A satisfies the equation $\frac{dA}{dt} + (\mathbf{u} \cdot \nabla)A = 0$, then \mathbf{C} satisfies the equation*

$$\frac{d\mathbf{C}}{dt} + (\mathbf{u} \cdot \nabla)\mathbf{C} = 0;$$

(b). *if A satisfies the equation $\frac{dA}{dt} + \frac{s}{2\lambda_1}A - (\nabla\mathbf{u})A = 0$, then \mathbf{C} satisfies the equation*

$$\frac{d\mathbf{C}}{dt} + \frac{s}{\lambda_1}\mathbf{C} - (\nabla\mathbf{u})\mathbf{C} - \mathbf{C}(\nabla\mathbf{u})^t = 0.$$

Proof: (a) Multiplying the equation by A^t to the right, and the transpose of the equation by A to the left, we have,

$$\frac{dA}{dt}A^t + (\mathbf{u} \cdot \nabla)AA^t = 0, \quad (L1)$$

$$A\frac{dA^t}{dt} + A(\mathbf{u} \cdot \nabla)A^t = 0, \quad (L2)$$

Adding (L1) and (L2) gives,

$$\frac{d(AA^t)}{dt} + (\mathbf{u} \cdot \nabla)(AA^t) = 0; \text{ that is, } \frac{d\mathbf{C}}{dt} + (\mathbf{u} \cdot \nabla)(\mathbf{C}) = 0.$$

(b) Multiplying the equation by A^t to the right, and the transpose of the equation by A to the left, we have,

$$\frac{dA}{dt}A^t + \frac{s}{2\lambda_1}AA^t - (\nabla \mathbf{u})AA^t = 0, \quad (L3)$$

$$A\frac{dA^t}{dt} + \frac{s}{2\lambda_1}AA^t - AA^t(\nabla \mathbf{u})^t = 0, \quad (L4)$$

Adding (L3) and (L4) gives,

$$\frac{d(AA^t)}{dt} + \frac{s}{\lambda_1}AA^t - (\nabla \mathbf{u})AA^t - AA^t(\nabla \mathbf{u})^t = 0,$$

or,

$$\frac{d\mathbf{C}}{dt} + \frac{s}{\lambda_1}\mathbf{C} - (\nabla \mathbf{u})\mathbf{C} - \mathbf{C}(\nabla \mathbf{u})^t = 0. \quad \square$$

Similarly, we can define finite dimensional spaces $\mathbf{V}_{A_{Lh}(t)}$ and $\mathbf{V}_{A_{0h}}$ for A . When applying the Lie's scheme to the discrete analogue of the problem (14)-(21) with the above factorization and equations for A and the backward Euler's method to some sub-problems, we obtain

$$\mathbf{u}^0 = \mathbf{u}_{0h}, \mathbf{C}^0 = \mathbf{C}_{0h}, \mathbf{G}^0 = \mathbf{G}_0, \mathbf{V}^0 = \mathbf{V}_0, \omega^0 = \omega_0 \text{ given}, \quad (29)$$

for $n \geq 0$, $\mathbf{u}^n, \mathbf{C}^n, \mathbf{G}^n, \mathbf{V}^n, \omega^n$ being known, we compute $\mathbf{u}^{n+\frac{1}{5}}$, and $p^{n+\frac{1}{5}}$ via the solution of

$$\begin{cases} \rho_f \int_{\Omega} \frac{\mathbf{u}^{n+\frac{1}{5}} - \mathbf{u}^n}{\Delta t} \cdot \mathbf{v} \, d\mathbf{x} - \int_{\Omega} p^{n+\frac{1}{5}} \nabla \cdot \mathbf{v} \, d\mathbf{x} = 0, \forall \mathbf{v} \in \mathbf{V}_{0h} \\ \int_{\Omega} q \nabla \cdot \mathbf{u}^{n+\frac{1}{5}} \, d\mathbf{x} = 0, \forall q \in L_h^2; \mathbf{u}^{n+\frac{1}{5}} \in \mathbf{V}_{\mathbf{g}_{0h}}^{n+1}, p^{n+\frac{1}{5}} \in L_{0h}^2. \end{cases} \quad (30)$$

Next, we compute $\mathbf{u}^{n+\frac{2}{5}}$ and $A^{n+\frac{2}{5}}$ via the solution of

$$\begin{cases} \rho_f \int_{\Omega} \frac{d\mathbf{u}(t)}{dt} \cdot \mathbf{v} \, d\mathbf{x} + \int_{\Omega} (\mathbf{u}^{n+\frac{1}{5}} \cdot \nabla) \mathbf{u}(t) \cdot \mathbf{v} \, d\mathbf{x} = 0, \forall \mathbf{v} \in \mathbf{V}_{0h}^{n+1,-}; \\ \mathbf{u}(t^n) = \mathbf{u}^{n+\frac{1}{5}}, \\ \mathbf{u}(t) \in \mathbf{V}_h, \mathbf{u}(t) = \mathbf{g}_{0h}(t^{n+1}) \text{ on } \Gamma^{n+1,-} \times [t^n, t^{n+1}]; \end{cases} \quad (31)$$

$$\begin{cases} \int_{\Omega} \frac{dA(t)}{dt} : \mathbf{s} \, d\mathbf{x} + \int_{\Omega} (\mathbf{u}^{n+\frac{1}{5}} \cdot \nabla) A(t) : \mathbf{s} \, d\mathbf{x} = 0, \forall \mathbf{s} \in \mathbf{V}_{A_{0h}}; \\ A(t^n) = A^n, \text{ where } A^n(A^n)^t = \mathbf{C}^n \\ A(t) \in \mathbf{V}_{A_{Lh}}^{n+1}, t \in [t^n, t^{n+1}]; \end{cases} \quad (32)$$

and set $\mathbf{u}^{n+\frac{2}{5}} = \mathbf{u}(t^{n+1})$ and $A^{n+\frac{2}{5}} = A(t^{n+1})$, where $\Gamma^{n+1,-} = \{\mathbf{x} \in \Gamma, \mathbf{g}_{0h}(t^{n+1})(\mathbf{x}) \cdot \mathbf{n}(\mathbf{x}) < 0\}$, $\mathbf{V}_h = \{\mathbf{v}_h | \mathbf{v}_h \in (C^0(\overline{\Omega}))^2, \mathbf{v}_h|_E \in (P_1)^2, \forall E \in \mathcal{T}_h, \}$, and $\mathbf{V}_{0h}^{n+1,-} = \{\mathbf{v} \in \mathbf{V}_h, \mathbf{v} = 0, \text{ on } \Gamma^{n+1,-}\}$.

Then, compute $\mathbf{u}^{n+\frac{3}{5}}$ and $A^{n+\frac{3}{5}}$ via the solution of

$$\begin{cases} \rho_f \int_{\Omega} \frac{\mathbf{u}^{n+\frac{3}{5}} - \mathbf{u}^{n+\frac{2}{5}}}{\Delta t} \cdot \mathbf{v} \, d\mathbf{x} + \alpha \mu \int_{\Omega} \nabla \mathbf{u}^{n+\frac{3}{5}} : \nabla \mathbf{v} \, d\mathbf{x} = 0, \\ \forall \mathbf{v} \in \mathbf{V}_{0h}; \mathbf{u}^{n+\frac{3}{5}} \in \mathbf{V}_{\mathbf{g}_{0h}}^{n+1}, \end{cases} \quad (33)$$

$$\begin{cases} \int_{\Omega} \left(\frac{A^{n+\frac{3}{5}} - A^{n+\frac{2}{5}}}{\Delta t} - (\nabla \mathbf{u}^{n+\frac{3}{5}}) A^{n+\frac{3}{5}} + \frac{f(A^{n+\frac{2}{5}}(A^{n+\frac{2}{5}})^t)}{2\lambda_1} A^{n+\frac{3}{5}} \right) : \mathbf{s} \, d\mathbf{x} = 0, \\ \forall \mathbf{s} \in \mathbf{V}_{A_{0h}}; A^{n+\frac{3}{5}} \in \mathbf{V}_{A_{Lh}}^{n+1}, \end{cases} \quad (34)$$

and set

$$\mathbf{C}^{n+\frac{3}{5}} = A^{n+\frac{3}{5}}(A^{n+\frac{3}{5}})^t + \frac{\Delta t}{\lambda_1} f(\mathbf{A}^{n+\frac{3}{5}}(\mathbf{A}^{n+\frac{3}{5}})^t) \mathbf{I}. \quad (35)$$

Then, predict the position and the translation velocity of the center of mass as follows:

Take $\mathbf{V}^{n+\frac{3}{5},0} = \mathbf{V}^n$ and $\mathbf{G}^{n+\frac{3}{5},0} = \mathbf{G}^n$; then predict the new position and translation velocity via the following sub-cycling and predicting-correcting technique

For $k = 1, 2, \dots, N$, compute

$$\hat{\mathbf{V}}^{n+\frac{3}{5},k} = \mathbf{V}^{n+\frac{3}{5},k-1} + (1 - \rho_f/\rho_s)^{-1} M_p^{-1} \mathbf{F}^r(\mathbf{G}^{n+\frac{3}{5},k-1}) \Delta t / 2N, \quad (36)$$

$$\hat{\mathbf{G}}^{n+\frac{3}{5},k} = \mathbf{G}^{n+\frac{3}{5},k-1} + (\Delta t / 4N)(\hat{\mathbf{V}}^{n+\frac{3}{5},k} + \mathbf{V}^{n+\frac{3}{5},k-1}), \quad (37)$$

$$\mathbf{V}^{n+\frac{3}{5},k} = \mathbf{V}^{n+\frac{3}{5},k-1} + (1 - \rho_f/\rho_s)^{-1} M_p^{-1} (\mathbf{F}^r(\hat{\mathbf{G}}^{n+\frac{3}{5},k}) + \mathbf{F}^r(\mathbf{G}^{n+\frac{3}{5},k-1})) \Delta t / 4N, \quad (38)$$

$$\mathbf{G}^{n+\frac{3}{5},k} = \mathbf{G}^{n+\frac{3}{5},k-1} + (\Delta t / 4N)(\mathbf{V}^{n+\frac{3}{5},k} + \mathbf{V}^{n+\frac{3}{5},k-1}), \quad (39)$$

end do; let $\mathbf{V}^{n+\frac{3}{5}} = \mathbf{V}^{n+\frac{3}{5},N}$, $\mathbf{G}^{n+\frac{3}{5}} = \mathbf{G}^{n+\frac{3}{5},N}$.

Next compute $\{\mathbf{u}^{n+\frac{4}{5}}, \boldsymbol{\lambda}^{n+\frac{4}{5}}, \mathbf{V}^{n+\frac{4}{5}}, \omega^{n+\frac{4}{5}}\}$ via the solution of

$$\begin{cases} \rho_f \int_{\Omega} \frac{\mathbf{u}^{n+\frac{4}{5}} - \mathbf{u}^{n+\frac{3}{5}}}{\Delta t} \cdot \mathbf{v} d\mathbf{x} + \beta \mu \int_{\Omega} \nabla \mathbf{u}^{n+\frac{4}{5}} : \nabla \mathbf{v} d\mathbf{x} \\ + (1 - \frac{\rho_f}{\rho_s}) \left[M_p \frac{\mathbf{V}^{n+\frac{4}{5}} - \mathbf{V}^{n+\frac{3}{5}}}{\Delta t} \cdot \mathbf{Y} + I_p \frac{\omega^{n+\frac{4}{5}} - \omega^n}{\Delta t} \cdot \theta \right] \\ = \langle \boldsymbol{\lambda}^{n+\frac{4}{5}}, \mathbf{v} - \mathbf{Y} - \theta \times \mathbf{G}^{n+\frac{3}{5}} \mathbf{x} \rangle_{B_h^{n+\frac{3}{5}}} + (1 - \rho_f/\rho_s) M_p \mathbf{g} \cdot \mathbf{Y}, \\ \forall \mathbf{v} \in \mathbf{V}_{0h}, \mathbf{Y} \in \mathbb{R}^2, \theta \in \mathbb{R}, \\ \langle \boldsymbol{\mu}, \mathbf{u}^{n+\frac{4}{5}} - \mathbf{V}^{n+\frac{4}{5}} - \omega^{n+\frac{4}{5}} \times \mathbf{G}^{n+\frac{3}{5}} \mathbf{x} \rangle_{B_h^{n+\frac{3}{5}}} = 0, \forall \boldsymbol{\mu} \in \boldsymbol{\Lambda}_h^{n+\frac{3}{5}}; \\ \mathbf{u}^{n+\frac{4}{5}} \in \mathbf{V}_{\mathbf{g}_{0h}}^{n+1}, \boldsymbol{\lambda}^{n+\frac{4}{5}} \in \boldsymbol{\Lambda}_h^{n+\frac{3}{5}}, \end{cases} \quad (40)$$

and set $\mathbf{C}^{n+\frac{4}{5}} = \mathbf{C}^{n+\frac{3}{5}}$, and then let $\mathbf{C}^{n+\frac{4}{5}} = \mathbf{I}$ in $B_h^{n+\frac{3}{5}}$.

Then take $\mathbf{V}^{n+1,0} = \mathbf{V}^{n+\frac{4}{5}}$ and $\mathbf{G}^{n+1,0} = \mathbf{G}^{n+\frac{3}{5}}$; and predict the final position and translation velocity as follows:

For $k = 1, 2, \dots, N$, compute

$$\hat{\mathbf{V}}^{n+1,k} = \mathbf{V}^{n+1,k-1} + (1 - \rho_f/\rho_s)^{-1} M^{-1} \mathbf{F}^r(\mathbf{G}^{n+1,k-1}) \Delta t / 2N, \quad (41)$$

$$\hat{\mathbf{G}}^{n+1,k} = \mathbf{G}^{n+1,k-1} + (\Delta t / 4N)(\hat{\mathbf{V}}^{n+1,k} + \mathbf{V}^{n+1,k-1}), \quad (42)$$

$$\mathbf{V}^{n+1,k} = \mathbf{V}^{n+1,k-1} + (1 - \rho_f/\rho_s)^{-1} M^{-1} (\mathbf{F}^r(\hat{\mathbf{G}}^{n+1,k}) + \mathbf{F}^r(\mathbf{G}^{n+1,k-1})) \Delta t / 4N, \quad (43)$$

$$\mathbf{G}^{n+1,k} = \mathbf{G}^{n+1,k-1} + (\Delta t / 4N)(\mathbf{V}^{n+1,k} + \mathbf{V}^{n+1,k-1}), \quad (44)$$

end do; let $\mathbf{V}^{n+1} = \mathbf{V}^{n+1,N}$, $\mathbf{G}^{n+1} = \mathbf{G}^{n+1,N}$.

Finally, compute \mathbf{u}^{n+1} via the solution of

$$\begin{cases} \rho_f \int_{\Omega} \frac{\mathbf{u}^{n+1} - \mathbf{u}^{n+\frac{4}{5}}}{\Delta t} \cdot \mathbf{v} d\mathbf{x} + \gamma \mu \int_{\Omega} \nabla \mathbf{u}^{n+1} : \nabla \mathbf{v} d\mathbf{x}, \\ = \frac{\eta}{\lambda_1} \int_{\Omega} \mathbf{v} \cdot (\nabla \cdot f(\mathbf{C}^{n+\frac{4}{5}})(\mathbf{C}^{n+\frac{4}{5}} - \mathbf{I})) d\mathbf{x}, \forall \mathbf{v} \in \mathbf{V}_{0h}; \mathbf{u}^{n+1} \in \mathbf{V}_{\mathbf{g}_{0h}}^{n+1}. \end{cases} \quad (45)$$

We complete the final step by setting $\mathbf{C}^{n+1} = \mathbf{C}^{n+\frac{4}{5}}$, and $\omega^{n+1} = \omega^{n+\frac{4}{5}}$.

In the above, \mathbf{u}_{0h} is an approximation of \mathbf{u}_0 so that $\int_{\Omega} q \nabla \cdot \mathbf{u}_{0h} d\mathbf{x} = 0$, $\forall q \in L_h^2$, $\mathbf{V}_{\mathbf{g}_{0h}}^{n+1} = \mathbf{V}_{\mathbf{g}_{0h}(t^{n+1})}$, $\boldsymbol{\Lambda}_h^{n+s} = \boldsymbol{\Lambda}_h(t^{n+s})$, $\mathbf{V}_{A_{Lh}}^{n+1} = \mathbf{V}_{A_{Lh}(t^{n+1})}$, $B_h^{n+s} = B_h(t^{n+s})$, the spaces $\mathbf{V}_{A_{Lh}(t)}$ and $\mathbf{V}_{A_{0h}}$ for \mathbf{A} are defined similar to those $\mathbf{C}_{Lh}(t)$ and \mathbf{C}_{0h} , and $\alpha + \beta + \gamma = 1$, for $\alpha, \beta, \gamma \geq 0$.

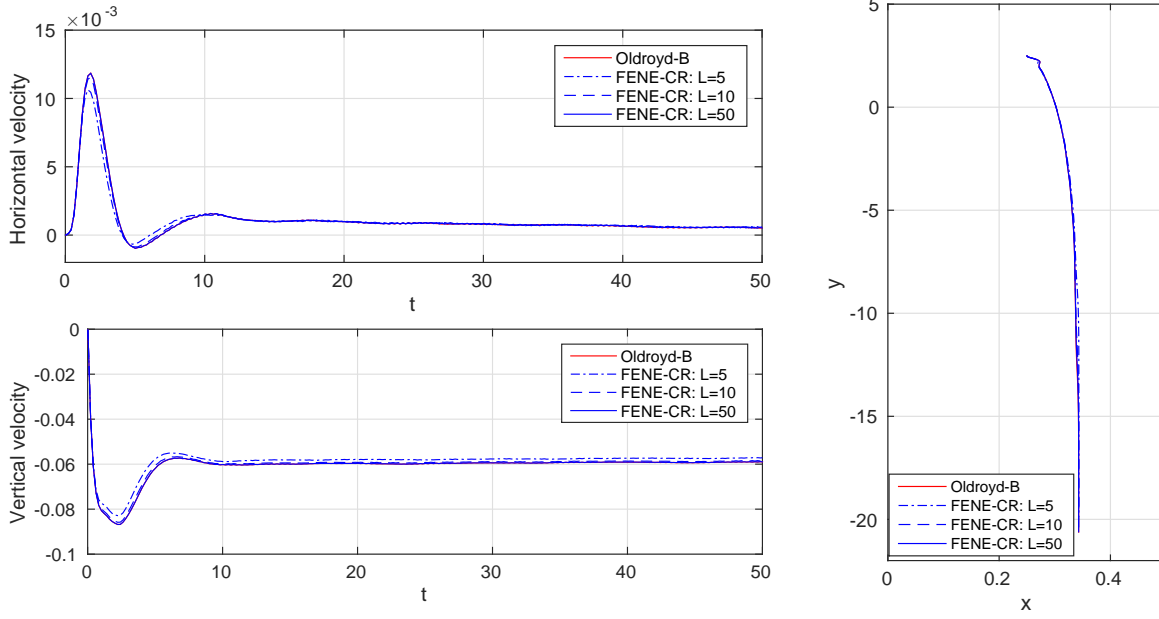


Figure 2: Histories of the particle horizontal velocity (left top), vertical velocity (left bottom) and trajectories of a disk (right) for $\lambda_1=2.025$ (the associated numbers are $Re=0.4186$, $M=0.4393$, $De=0.4611$, $E=1.1016$ for Oldroyd-B fluid and $Re=0.4059$, $M=0.4261$, $De=0.4472$, $E=1.1016$ for FENE-CR fluid of $L=5$).

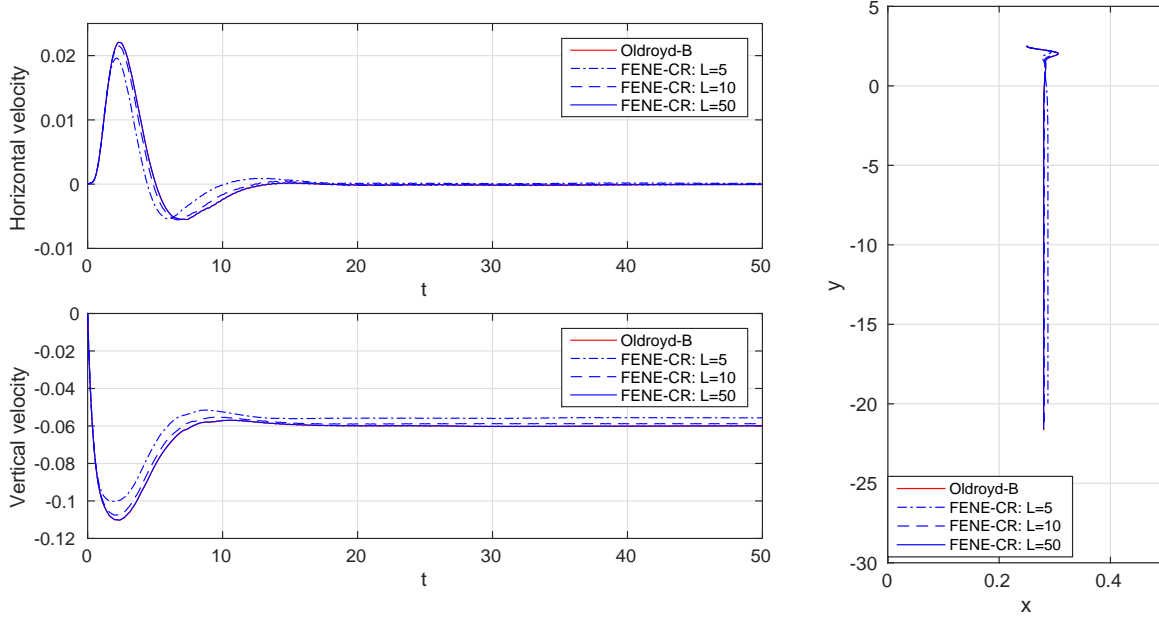


Figure 3: Histories of the particle horizontal velocity (left top), vertical velocity (left bottom) and trajectories of a disk (right) for $\lambda_1=4.05$ (the associated numbers are $Re=0.4403$, $M=0.6536$, $De=0.9701$, $E=2.2032$ for Oldroyd-B fluid and $Re=0.4110$, $M=0.6101$, $De=0.9056$, $E=2.2032$ for FENE-CR fluid of $L=5$).

2.4 Solution strategies

In the algorithm (29)-(45), we have obtained a sequence of simpler sub-problems, namely: (i) using a L^2 -projection Stokes solver à la Uzawa to force the incompressibility condition in (30), (ii) an advection step for the velocity and conformation tensor in (31) and (32), (iii) a diffusion step for the velocity in (33) and the step for the rest of the constitutive equations for the conformation tensor in (34) and (35), (iv) a step to predict the particle position in (36)-(39), (v) a step to enforce the rigid body motion inside the particle and to obtain its updated translation and angular velocity in (40) and then to set the conformation tensor to be an identity matrix inside the particle, (vi) a step to correct the particle position in (41)-(44), and (vii) a diffusion step with the updated polymeric stress tensor for the velocity in (45).

The resulting methodology is easy to implement and quite modular. A degenerated quasi-Stokes problem (30) is solved by an Uzawa/ preconditioned conjugate gradient algorithm operating in the space L^2_{0h} discussed in [11] and [18]. The advection problems (31) and (32) are solved by a wave-like equation method (see [18] and [19]) which is an explicit method and does not introduce numerical dissipation. Since the advection problem is decoupled from the other ones, we can choose a proper sub-time step so that the CFL condition is satisfied. Problem (40), concerning the rigid body motion enforcement, is a saddle point problem and is solved by a conjugate gradient method given in e.g., [11] and [18]. Problems (33) and (45) are classical elliptic problems which can be solved by a matrix-free fast solver. In (36)-(39) and (41)-(44), it is a predicting-correcting scheme to obtain the position of the mass center and the translation velocity of the particle. Problem (34) gives a simple equation at each grid point which can be solved easily if we use the trapezoidal quadrature rule to compute the integrals as in [11].

3 Numerical Results and discussion

To study the effect of the polymer extension limit L on the particle chain formation while settling, we have considered the cases of two, three and six disks settling in viscoelastic fluid as in [11] since vertical chains are known to be formed for these cases. The computational results for disks settling in Oldroyd-B fluid are obtained by the numerical method developed in [11] and these results are compared with those results obtained by the scheme discussed in the previous section for the FENE-CR model at large values of L for validation purpose since $f(\mathbf{C}) = \frac{L^2}{L^2 - tr(\mathbf{C})} \rightarrow 1$ as $L \rightarrow \infty$ (i.e., the FENE-CR model has almost recovered the Oldroyd-B model for the large values of L). In the following discussion, the particle Reynolds number is $Re = \frac{\rho_f U d}{\eta_1}$, the Debra number is $De = \frac{\lambda_1 U}{d}$, the Mack number is $M = \sqrt{De Re}$, and the elasticity number is $E = De / Re = \frac{\lambda_1 \eta_1}{d^2 \rho_f}$ where U is the averaged terminal speed of disks and d is the disk diameter.

3.1 Few settling disks

We have first considered the settling of one disk in a vertical channel of infinite length filled with a viscoelastic fluid as in [11], the computational domain is $\Omega = (0, 1) \times (0, 6)$ initially and then it moves vertically with the mass center of the disk (see, e.g., [20] and [21] and references therein for adjusting the computational domain according to the position of the particle). The disk diameter is $d = 0.25$ and the initial position of the disk center is at $(0.25, 2.5)$. The disk density ρ_s is 1.0007 and the fluid density ρ_f is 1. The fluid viscosity η_1 is 0.034. The relaxation time λ_1 is either 2.025 or 4.05 and the retardation time λ_2 is $\lambda_1/8$. Hence the values of the elasticity number E are 1.1016 and 2.2032 for $\lambda_1 = 2.025$ and 4.05, respectively. The maximal polymer extension L is either 5, 10, or 50 for the FENE-CR model. The mesh sizes for the velocity field, conformation tensor and pressure are $h = 1/128$, $1/128$, and $1/64$, respectively; and the time step is 0.0004. Fig. 2 shows that the trajectories of a disk settling in either Oldroyd-B or FENE-CR fluids are almost identical for $L=5$, 10, and 50 and $\lambda_1 = 1.1016$ ($E=1.1016$); but in Fig. 3 the disk trajectory for $L=5$

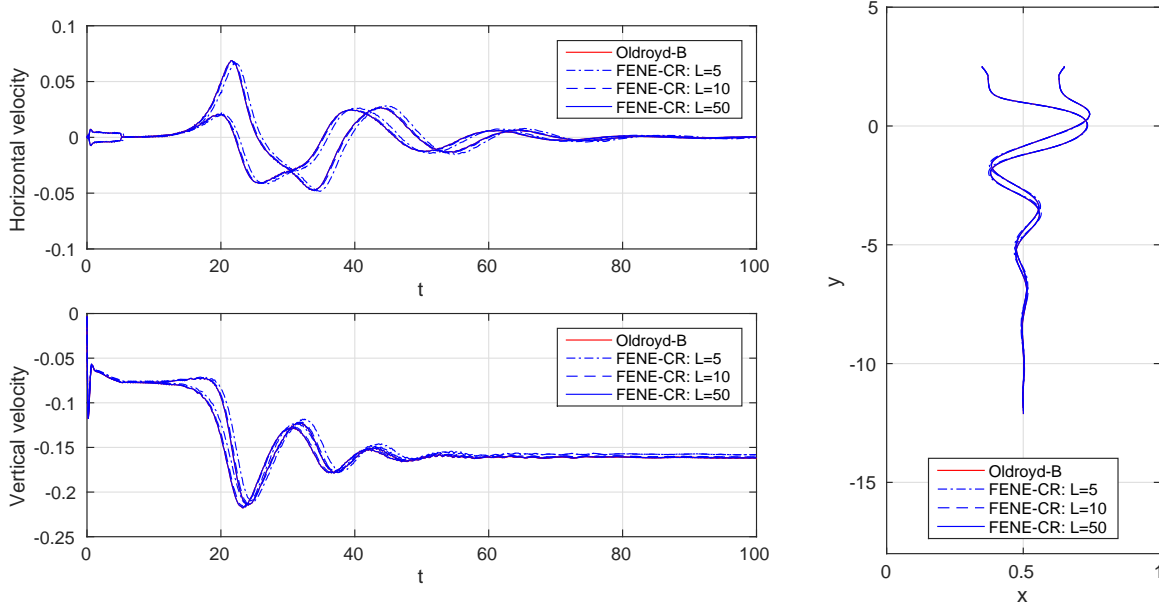


Figure 4: Histories of the particle horizontal velocity (left top), vertical velocity (left bottom) and trajectories of two disks (right) for $\lambda_1=0.5$ (the associated numbers are $Re=0.202$, $M=0.255$, $De=0.323$, $E=1.6$ and $Re=0.197$, $M=0.249$, $De=0.316$, $E=1.6$ for Oldroyd-B fluid and FENE-CR of $L=5$, respectively).

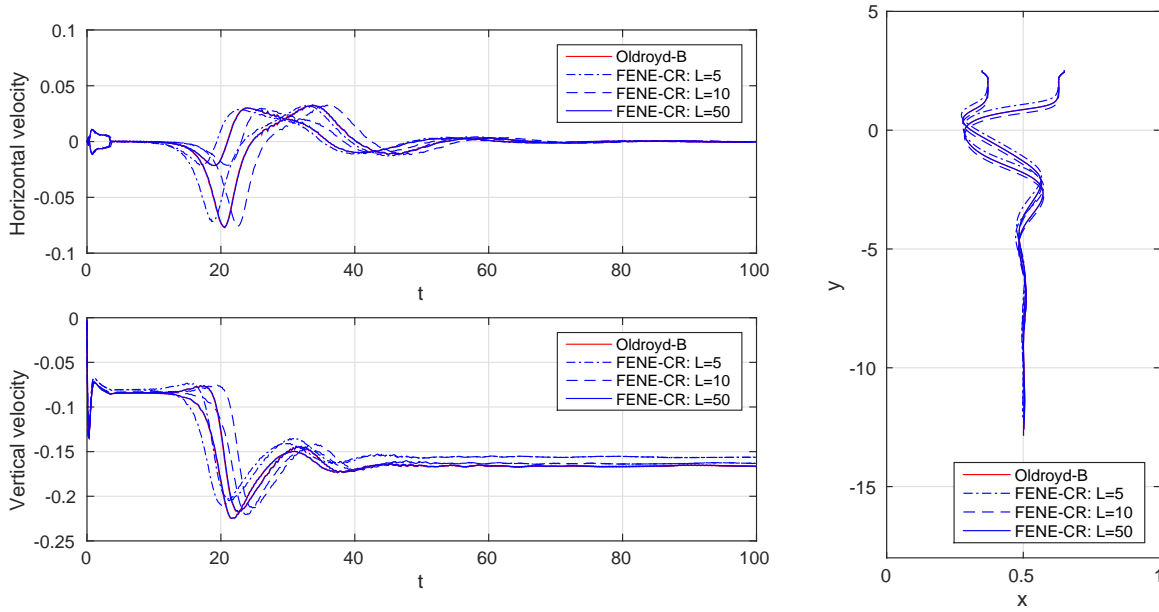


Figure 5: Histories of the particle horizontal velocity (left top), vertical velocity (left bottom) and trajectories of two disks (right) for $\lambda_1=1$ (the associated numbers are $Re=0.208$, $M=0.371$, $De=0.664$, $E=3.2$ and $Re=0.195$, $M=0.35$, $De=0.625$, $E=3.2$ for Oldroyd-B fluid and FENE-CR of $L=5$, respectively).

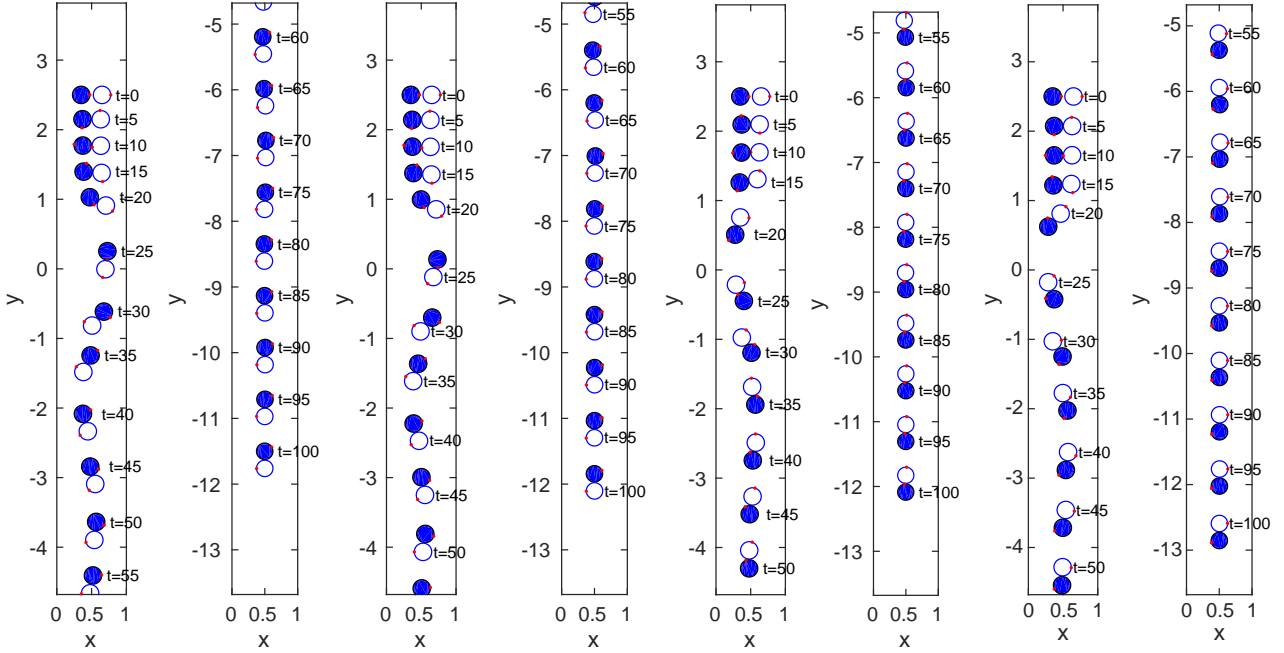


Figure 6: Positions of two disks : FENE-CR of $L = 5$ and $\lambda_1 = 0.5$ (left two), Oldroyd-B and $\lambda_1 = 0.5$ (middle left two), FENE-CR of $L = 5$ and $\lambda_1 = 1$ (middle right two), and Oldroyd-B and $\lambda_1 = 1$ (right two).

and $\lambda_1 = 4.05$ is quite different from those for $L = 10$ and 50 and $\lambda_1 = 4.05$ and that for Oldroyd-B fluid. For $\lambda_1 = 4.05$ ($E=2.2032$), the disk trajectory for $L=5$ is different from others is due to that its Deborah number is slightly smaller (actually the values of associated De are 0.9056 , 0.9519 , 0.9693 , and 0.9701 for the FENE-CR fluid for $L=5$, 10 , 50 , and Oldroyd-B). As observed in [22], the effect of Deborah number on the single particle settling trajectory is that the smaller De is, the closer to the center line the equilibrium position is. Histories of the particle horizontal velocity, vertical velocity and trajectories of a disk obtained for this one disk case show that the larger value of polymer extension limit L is, the closer to the those of a disk settling in Oldroyd-B fluid is.

For the cases of two disks sedimenting in a vertical channel of infinite length filled with a viscoelastic fluid, the computational domain is $\Omega = (0, 1) \times (0, 6)$ initially and then it moves vertically with the mass center of the lower disk between two disks. The two disk diameters are $d = 0.25$ and the initial position of the disk centers are at $(0.35, 2.5)$ and $(0.65, 2.5)$, respectively. The disk density ρ_s is 1.01 and the fluid density ρ_f is 1 . The fluid viscosity η_1 is 0.2 . The relaxation time λ_1 is either 0.5 or 1 and the retardation time λ_2 is $\lambda_1/4$. Hence the elasticity number E are 1.6 and 3.2 for $\lambda_1 = 0.5$ and 1 , respectively. The maximal polymer extension L is either 5 , 10 , or 50 for the FENE-CR model. The mesh sizes for the velocity field, conformation tensor and pressure are $h = 1/96$, $1/96$, and $1/48$, respectively; and the time step is 0.0004 . Fig. 4 shows that the trajectories of two disks settling in either Oldroyd-B or FENE-CR fluids are almost identical for $\lambda_1 = 0.5$ and $L=5$, 10 , and 50 . Similar behaviors are also observed for the vertical and horizontal particle translation velocities shown in Figs. 4. But, in Fig. 5, the two disk trajectories for $\lambda_1 = 1$ and $L=5$ and 10 are slightly different from those for $\lambda_1 = 1$ and $L = 50$ and those for Oldroyd-B fluid. Similar behaviors for the cases of $L=5$ and 10 are also observed for the vertical and horizontal particle translation velocities shown in Fig. 5. For all cases, two disks attract to each other first, form a horizontal chain and then its broadside is turn into the falling direction; it is different from the well known phenomenon called drafting, kissing and

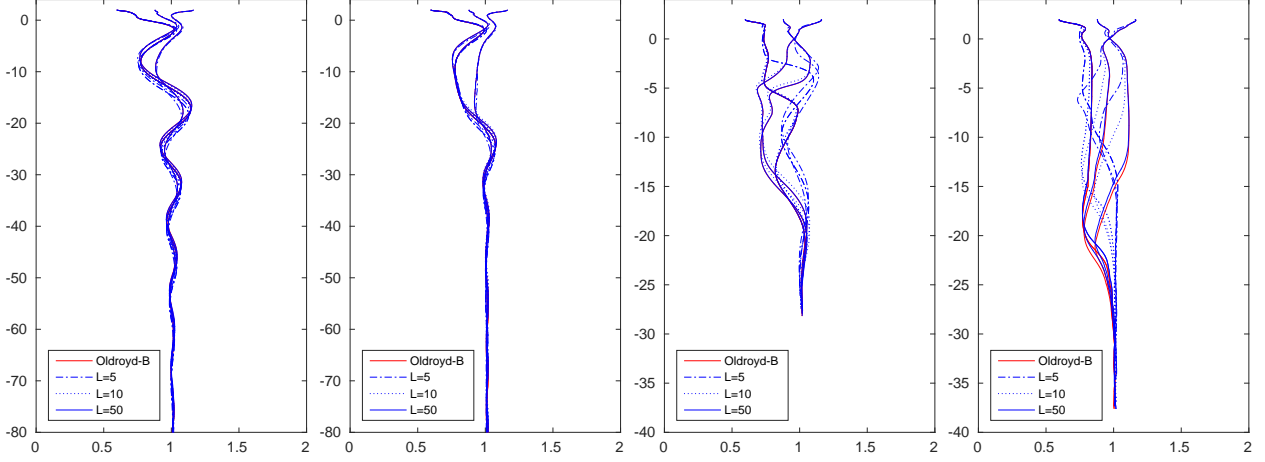


Figure 7: The disk trajectories: $\rho_s = 1.0075$ and $\lambda_1 = 0.75$ (left), $\rho_s = 1.01$, $\lambda_1 = 0.75$ (middle left), $\rho_s = 1.0075$, $\lambda_1 = 1.5$ (middle right), and $\rho_s = 1.01$, $\lambda_1 = 1.5$ (right).

tumbling for disks settling in Newtonian fluid [23]. In the position snapshots shown in Fig. 6, for the case of $L = 5$ and $E = 1.6$ two disks move slowest due to the smaller relaxation time and shorter extension value of L and, on the other hand, for the case of Oldroyd-B fluid and $E = 3.2$, two disks move further down in the channel. But for the both cases of $L = 50$, the particle motions are almost identical to those in Oldroyd-B fluid as in Figs. 4 and 5.

For the cases of three disks sedimenting in a vertical channel of infinite length filled with a viscoelastic fluid, the computational domain is $\Omega = (0, 2) \times (0, 5)$ initially and then it moves vertically with the mass center of the lowest disk among three disks. The three disk diameters are $d = 0.25$ and the initial disk centers are $(0.6, 2)$, $(0.88, 2)$ and $(1.16, 2)$, respectively. The disk density ρ_s is either 1.0075 or 1.01 and the fluid density ρ_f is 1. The fluid viscosity η_1 is 0.26. The relaxation time λ_1 is either 0.75 or 1.5 and the retardation time λ_2 is $\lambda_1/8$. Hence the elasticity number E are 3.12 and 6.24 for $\lambda_1 = 0.75$ and 1.5, respectively. The maximal polymer extension L is either 5, 10, or 50 for the FENE-CR model. The mesh sizes for the velocity field, conformation tensor and pressure are $h = 1/96$, $1/96$, and $1/48$, respectively; and the time step is 0.0004. Fig. 7 shows that the trajectories of three disks of both densities settling in either Oldroyd-B or FENE-CR fluids are close to each other for $E = 3.12$, $L = 10$ and 50. But at $E = 6.24$, the three disk trajectories for $L = 5$ are very different from those for $L = 50$ and those for Oldroyd-B fluid. For all cases shown in Figs. 8 and 9, the middle disk moves downward faster first and the other two are drafted toward this leading disk. Then they rearrange themselves and form a curved chain. Finally the curved chain straighten out due to the large normal stress next to the middle disk in the curved chain (as discussed in [24]). For the cases of $L = 50$, the particle trajectories are almost identical to those of Oldroyd-B fluid as in Fig. 7.

The above numerical results suggest that the effect of the shorter extensibility in the FENE-CR model on the particle settling trajectory can be enhanced by increasing the value of relaxation time λ_1 . It is known that when the elasticity number $E = De/Re$ is larger than the critical value ($O(1)$) and the Mach number $M = \sqrt{De/Re}$ is less than the critical value, the long particle settling in an Oldroyd-B fluid can turn its broadside parallel to the falling direction ([24], [25]). For two disk and three disk cases considered in this section, the values of the elasticity number are large than the critical values and those of the Mach number are smaller than 1 and particle chain is always formed with its “broadside” parallel parallel to the flow direction. Thus, at least for the cases and the values of L considered in this section, we have obtained that the polymer extension limit L has no effect on a short vertical chain formation of particles; but the

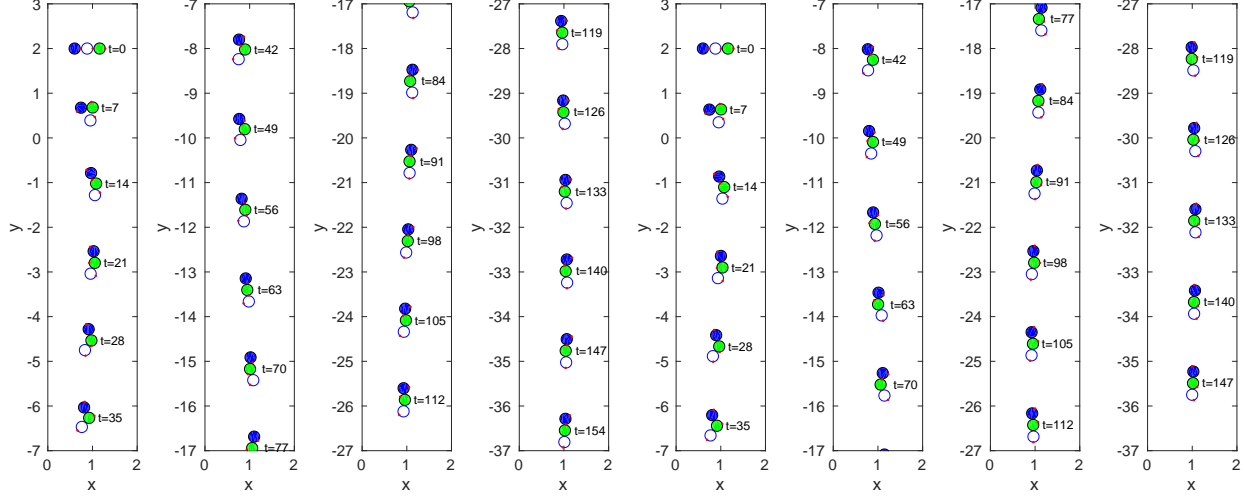


Figure 8: Positions of three disks for $\rho_s = 1.0075$: FENE-CR of $L = 5$ & $\lambda_1 = 0.75$, $\text{Re}=0.244$, $\text{M}=0.431$, $\text{De}=0.762$, and $\text{E}=3.12$ (left four) and Oldroyd-B & $\lambda_1 = 0.75$, $\text{Re}=0.259$, $\text{M}=0.440$, $\text{De}=0.777$, $\text{E}=3.12$ (right four).

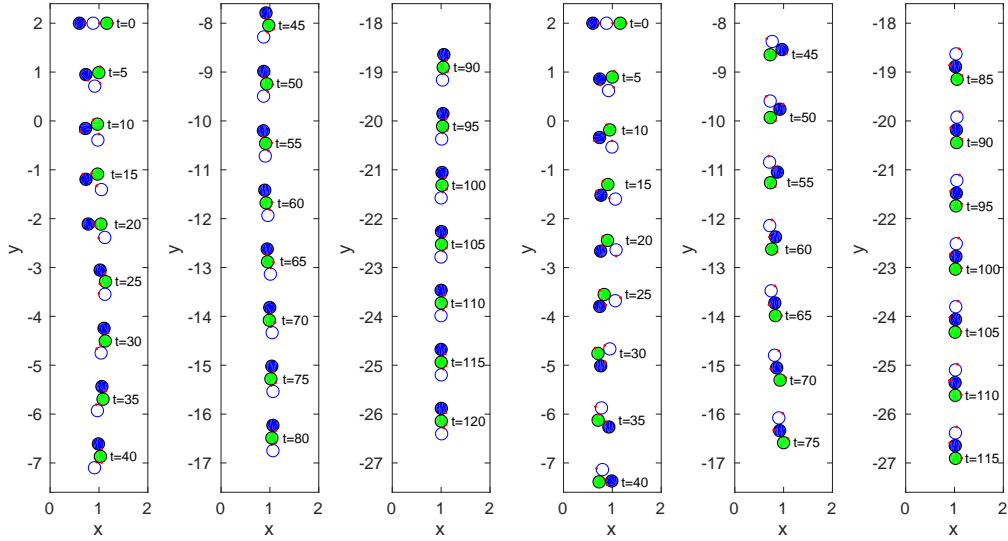


Figure 9: Positions of three disks for $\rho_s = 1.0075$: FENE-CR of $L = 5$ & $\lambda_1 = 1.5$, $\text{Re}=0.232$, $\text{M}=0.579$, $\text{De}=1.447$, $\text{E}=6.24$ (left three) and Oldroyd-B & $\lambda_1 = 1.5$, $\text{Re}=0.248$, $\text{M}=0.620$, $\text{De}=1.550$, $\text{E}=6.24$ (right three).

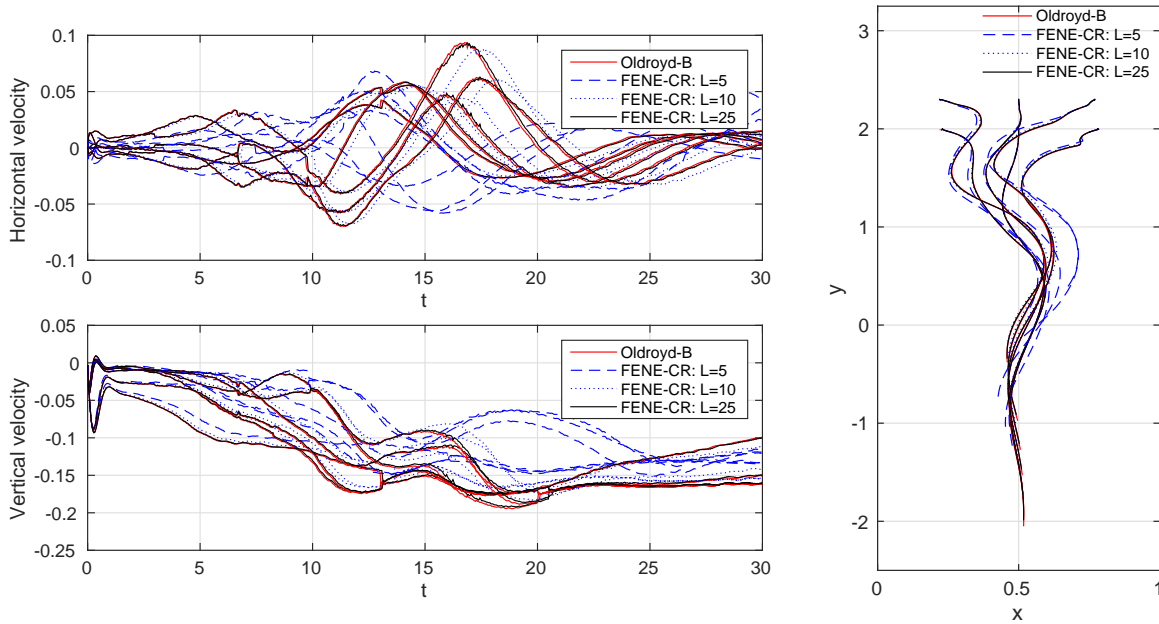


Figure 10: Histories of the particle velocity (left) and trajectories of six disks (right) for $\lambda_1=1.3$.

intermediate dynamics of particle interaction before having a vertical chain can be different for smaller values of L when increasing the relaxation time λ_1 .

3.2 Several settling disks

To find out the effect of the polymer extension limit L on the formation of a long chain of particles, the first case in this section concerns six disks of diameter $d=0.25$ sedimenting in a channel filled with either an Oldroyd-B fluid or a FENE-CR fluid of viscosity $\eta_1=0.26$. The channel is infinitely long and has a width of 1. The computational domain is $\Omega = (0, 1) \times (0, 7)$ initially and then moves down with the mass center of the lowest of the six particles. The initial positions of the disks are $(0.23, 2.0)$, $(0.5, 2.0)$, $(0.78, 2.0)$, $(0.22, 2.30)$, $(0.5, 2.3)$, and $(0.77, 2.3)$. The disk density is $\rho_s=1.01$ and the fluid density is $\rho_f=1$. The relaxation time and retardation time are $\lambda_1=1.3$ and $\lambda_2 = \lambda_1/8$, respectively. The mesh sizes for the velocity field, conformation tensor and pressure are $h = 1/96$, $1/96$, and $1/48$, respectively; and the time step is 0.0004. In our simulations, all six particles in an Oldroyd-B fluid are lined up along the flow direction, agreeing thus the known observations and experiments. Fig. 11 gives the snapshots at various moments of time of the particles lining up phenomenon. We can see that, after drafting, kissing and chaining, the six particles form approximately a straight line at $t = 20$. Then a chain of 5 disks is maintained from $t = 22$ to 28; and at the same time duration the trailing particle has been separated from the leading five particles. This observation agrees with experiments showing that, sometimes, the last particle in the chain gets detached as discussed in [26]. It is known that a long chain falls faster than a single particle in the fluid. This long body effect tends to detach the last particle from the chain. The average terminal velocity is 0.1535 for $26 \leq t \leq 30$, the Reynolds number is $Re=0.1476$, the Deborah number is $De=0.7981$, the elasticity number is $E=5.408$ and the Mach number is $M=0.3432$. For the FENE-CR model for the polymer extension limit $L = 5$, since the viscoelastic fluid has a shorter polymer extension limit, it can not hold all six disks together as shown in Fig. 11 for $t \geq 16$; but instead two chains of three disks are formed and maintained. For this case, the average terminal velocity is 0.1317 for $26 \leq t \leq 30$, and the associated numbers are $Re=0.1266$, $De=0.6847$,

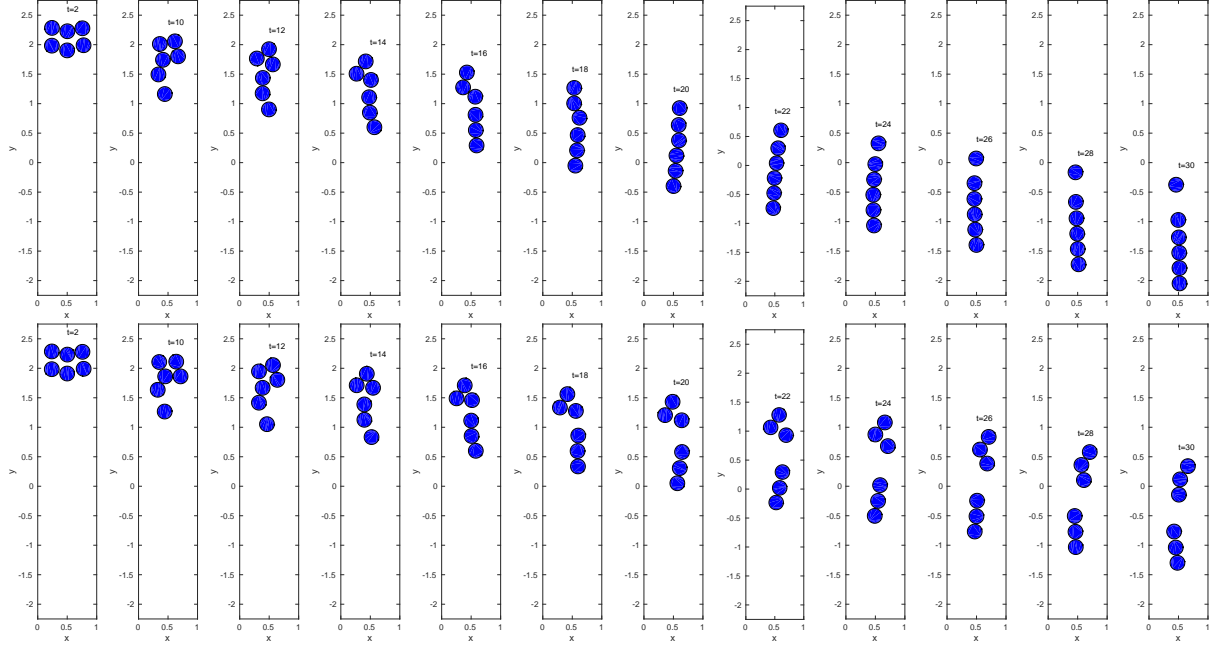


Figure 11: Snapshots of the positions of six disks at $t = 2, 10, 12, 14, 16, 18, 20, 22, 24, 26, 28$, and 30 for $\lambda_1=1.3$ in an Oldroyd-B fluid (top) and a FENE-CR fluid with $L = 5$ (bottom).

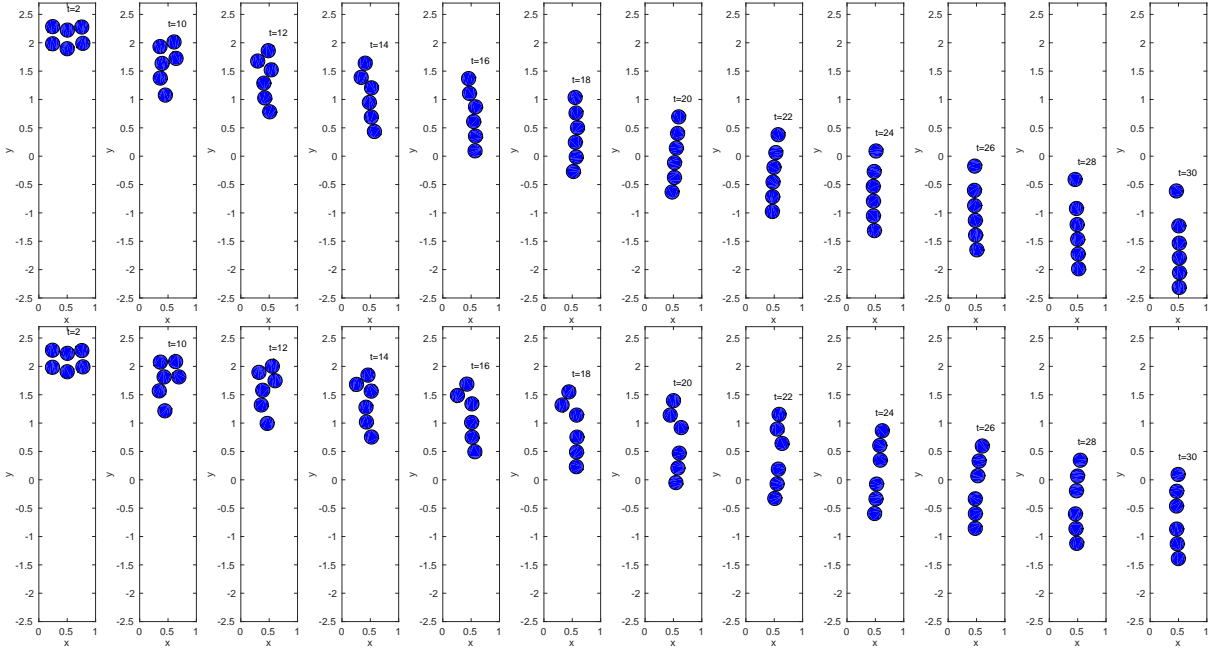


Figure 12: Snapshots of the positions of six disks at $t = 2, 10, 12, 14, 16, 18, 20, 22, 24, 26, 28$, and 30 for $\lambda_1=1.5$ in an Oldroyd-B fluid (top) and a FENE-CR fluid with $L = 5$ (bottom) and the associated numbers are $\text{Re}=0.149$, $\text{M}=0.3721$, $\text{De}=0.9295$, $\text{E}=6.24$ and $\text{Re}=0.1278$, $\text{M}=0.3194$, $\text{De}=0.7978$, $\text{E}=6.24$ for Oldroyd-B fluid and FENE-CR of $L=5$, respectively.

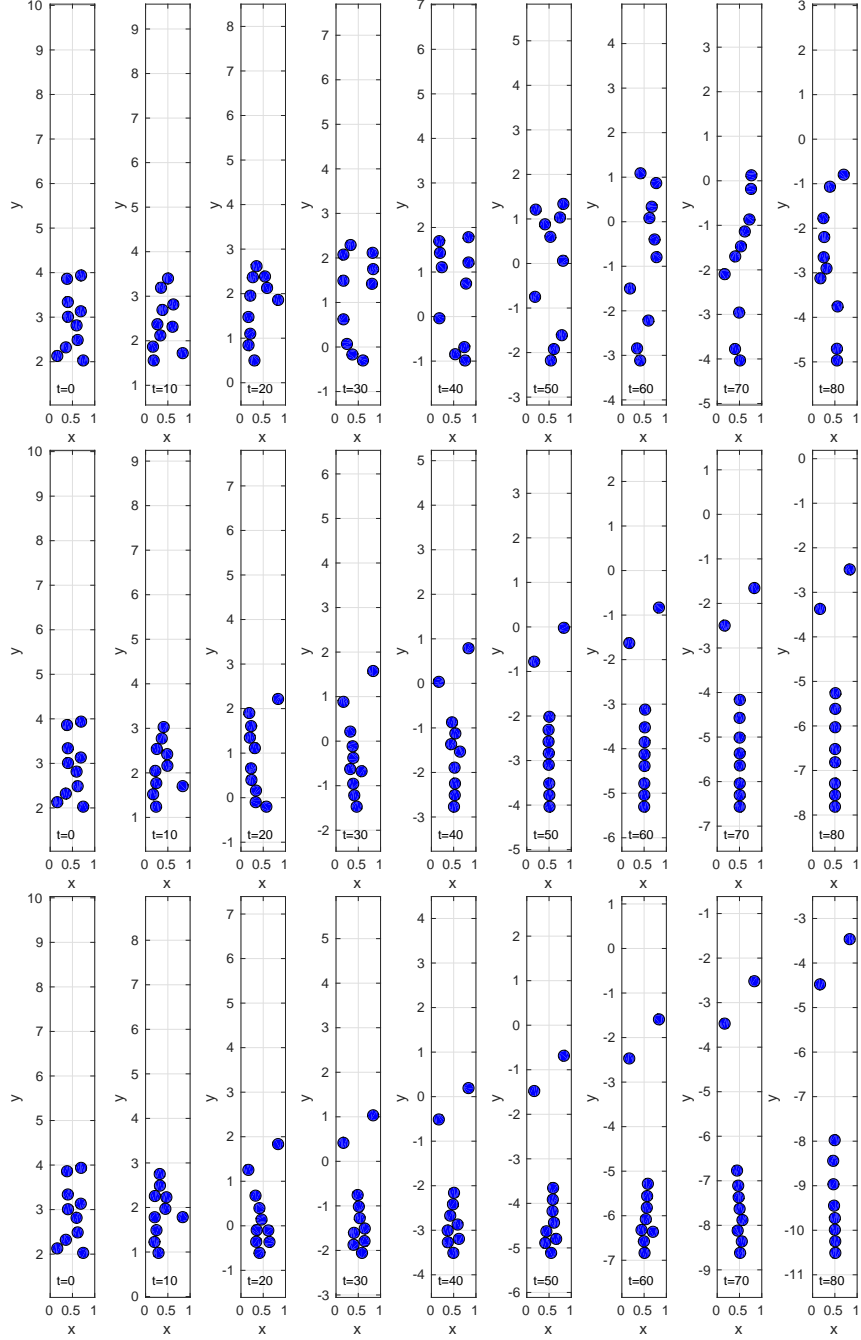


Figure 13: Snapshots of the positions of ten disks at $t = 0, 10, 20, 30, 40, 50, 60, 70$ and 80 in FENE-CR fluid for $L = 2$ (top) and $L = 5$ (middle) and in Oldroyd-B fluid (bottom). The associated numbers are $\text{Re}=0.1539, \text{M}=0.4439, \text{De}=1.2804, \text{E}=8.32$ for Oldroyd-B fluid; $\text{Re}=0.09626, \text{M}=0.2777, \text{De}=0.8009, \text{E}=8.32$ for FENE-CR fluid and $L=2$, and $\text{Re}=0.1092, \text{M}=0.3150, \text{De}=0.9085, \text{E}=8.32$ for FENE-CR fluid and $L=5$.

$E=5.408$, and $M=0.2944$. The particle velocities and trajectories for different values of L and $\lambda_1 = 1.3$ in Fig. 10 show that, as L is about 25, the dynamics of six disks in FENE-CR fluid is almost identical to the one in Oldroyd-B fluid. For slightly larger $\lambda_1 = 1.5$, the particle dynamics and chain formation are similar to those for $\lambda_1 = 1.3$; however those chains of disks in Fig. 12 are straighten out faster comparing to those in Fig. 11 by stronger normal stress due to the larger value of E .

In the second case of this section, we have increased the number of disks to ten and have kept all other parameters the same except that the computational domain is $\Omega = (0, 1) \times (0, 16)$, the relaxation time is $\lambda_1=2$ ($E=8.32$), and the ten disk mass centers are randomly chosen in the region $(0, 1) \times (2, 4)$ initially. This initial position give us some computational results concerning the effect of polymer extension limit L on the agglomeration and chain of particles. Fig. 13 is obtained for Oldroyd-B and FENE-CR viscoelastic fluids, respectively. In Oldroyd-B fluid, the positions of 10 disks at different instants of time show that the agglomeration of particles can be held initially in a cluster of 8 disks for $20 \leq t \leq 60$; but after the cluster becomes a long chain around $t = 70$, the formation of a long chain can not be kept due to the detachment of the trailing particle as discussed in the previous case of six disks. The results of the ten particles settling in an FENE-CR for $L = 2$ are quite different from those in Oldroyd-B fluid. All disks spread out most of time. The results of the ten particles settling in an FENE-CR for $L = 5$ are different from the those in Oldroyd-B fluid since these particles are still relatively easier to break away from the chains and clusters. There are two clusters for $20 \leq t \leq 40$; once the disks in these two clusters all line up, the last disk in the chain of more than 3 disks keep breaking away. The numerical results of three cases suggest that for smaller values of L , the length of the vertical chain is shorter and the size of cluster is smaller.

4 Conclusion

In this article we present a numerical method for simulating the sedimentation of circular particles in two-dimensional channel filled with a viscoelastic fluid of FENE-CR type, which is generalized from a domain/distributed Lagrange multiplier method with a factorization approach for Oldroyd-B fluids developed in [11]. Numerical results on the vertical chain formation suggest that the polymer extension limit L for the FENE-CR fluid has no effect on the cases of two disks and three disks in two-dimensional narrow channel, at least for the values of L considered in this article; but the intermediate dynamics of particle interaction before having a vertical chain can be different for smaller values of L when increasing the relaxation time. For six particles sedimenting in FENE-CR type viscoelastic fluid, the formation of disk chains does depend on the polymer extension limit L . For the smaller values of L , two chains of three disks are formed since FENE-CR type viscoelastic fluid can not bring them together like the case of these particles settling in a vertical chain formation in Oldroyd-B fluid. Similar results for the case of ten disks are also obtained. The numerical results of several more particle cases suggest that for smaller values of L , the length of the vertical chain is shorter and the size of cluster is smaller. The next step is to generalize this method to simulate cases of balls sedimenting in a three-dimensional channel filled with either kinds of viscoelastic fluid and to study the effect of the elasticity number on the length of particle chain and the size of particle clusters.

Acknowledgments.

We acknowledge the support of NSF (grant DMS-1418308).

References

- [1] R. P. Chhabra. Bubbles, Drops, and Particles in Non-Newtonian Fluids. CRC Press, Boca Raton, FA (1993)

- [2] G. H. McKinley. Steady and transient motion of spherical particles in viscoelastic liquids. In: D. De Kee and R. P. Chhabra (eds.) *Transport Processes in Bubbles, Drops & Particles*, 2nd ed., pp. 338-375. Taylor & Francis, New York, NY (2002)
- [3] M. J. Economides and K. G. Nolte. *Reservoir Stimulation*. Prentice Hall, Englewood Cliffs, NJ (1989)
- [4] I. Tomac and M. Gutierrez. Micromechanics of proppant agglomeration during settling in hydraulic fractures. *J. Petrol. Explor. Prod. Technol.*, **5**, 417-434 (2015).
- [5] F. P. T. Baaijens. Mixed finite element methods for viscoelastic flow analysis: A review. *J. Non-Newtonian Fluid Mech.*, **79**, 361-385 (1998)
- [6] R. Keunings. A survey of computational rheology. In: D. M. Binding et al. (eds.) *Proc. 13th Int. Congr. on Rheology*, Vol. 1, pp. 7-14. British Society of Rheology, Glasgow (2000)
- [7] R. Fattal and R. Kupferman. Constitutive laws for the matrix-logarithm of the conformation tensor. *J. Non-Newtonian Fluid Mech.*, **123**, 281-285 (2004)
- [8] R. Fattal and R. Kupferman. Time-dependent simulation of viscoelastic flows at high Weissenberg number using the log-conformation representation. *J. Non-Newtonian Fluid Mech.*, **126**, 23-37 (2005)
- [9] Y.-L. Lee and J. Xu. New formulations, positivity preserving discretizations and stability analysis for non-Newtonian flow models. *Comput. Methods Appl. Mech. Eng.*, **195**, 1180-1206 (2006)
- [10] A. Lozinski and R.G. Owens. An energy estimate for the Oldroyd-B model: theory and applications. *J. Non-Newtonian Fluid Mech.*, **112**, 161-176 (2003)
- [11] J. Hao, T.-W. Pan, R. Glowinski, and D. D. Joseph. A fictitious domain/distributed Lagrange multiplier method for the particulate flow of Oldroyd-B fluids: A positive definiteness preserving approach. *J. Non-Newtonian Fluid Mech.*, **156**, 95-111 (2009)
- [12] J. M. Rallison and E. J. Hinch. Do we understand the physics in the constitutive equation?. *J. Non-Newtonian Fluid Mech.*, **29**, 37-55 (1988)
- [13] D. D. Joseph. *Fluid Dynamics of Viscoelastic Liquids*. Springer, New York, NY (1990)
- [14] M. D. Chilcott and J. M. Rallison. Creeping flow of dilute polymer solutions past cylinders and spheres. *J. Non-Newtonian Fluid Mech.*, **29**, 381-432 (1988)
- [15] R. Glowinski, T.-W. Pan, T. I. Hesla, D. D. Joseph, and J. Périaux. A fictitious domain approach to the direct numerical simulation of incompressible viscous fluid flow past moving rigid bodies: application to particulate flow. *J. Comput. Phys.*, **169**, 363-426 (2001)
- [16] P. Singh, D. D. Joseph, T. I. Helsa, R. Glowinski, and T.-W. Pan. A distributed Lagrange multiplier/fictitious domain method for viscoelastic particulate flows. *J. Non-Newtonian Fluid Mech.*, **91**, 165-188 (2000)
- [17] A. J. Chorin, T. J. R. Hughes, M. F. McCracken, and J. E. Marsden, Product formulas and numerical algorithms, *Comm. Pure Appl. Math.*, **31**, 205-256 (1978).
- [18] R. Glowinski. Finite element methods for incompressible viscous flow. In *Handbook of Numerical Analysis*, edited by P. G. Ciarlet and J.-L. Lions (North-Holland, Amsterdam, 2003), Vol. IX, pp. 3-1976.
- [19] E. J. Dean and R. Glowinski. A wave equation approach to the numerical solution of the Navier-Stokes equations for incompressible viscous flow. *C.R. Acad. Sci. Paris, Série I*, t. **325**, 783-791 (1997)

- [20] H.H. Hu, D. D. Joseph, M. J. Crochet. Direct simulation of fluid particle motions. Theoret. Comput. Fluid Dynamics, **3**, 285-306 (1992).
- [21] T.-W. Pan, R. Glowinski, G. P. Galdi. Direct simulation of the motion of a settling ellipsoid in Newtonian fluid. J. Comput. Applied Math., **149**, 71-82 (2002).
- [22] J. Feng, P. Y. Huang, D. D. Joseph. Dynamicc simulation of sedimentation of solid particles in an Oldroyd-B fluid. J. Non-Newtonian Fluid Mech., **63**, 63-88 (1996)
- [23] A. F. Fortes, D. D. Joseph, and T. S. Lundgren. Nonlinear mechanics of fluidization of beds of spherical particles. J. Fluid Mech., **177**, 467-483 (1987)
- [24] P. Y. Huang, H. H. Hu, and D. D. Joseph. Direct simulation of the sedimentation of elliptic particles in Oldroyd-B fluids. J. Fluid Mech., **362**, 297-325 (1998)
- [25] Y. L. Liu, and D. D. Joseph. Sedimentation of particles in polymer solutions. J. Fluid Mech., **255**, 565-595 (1993)
- [26] N. A. Patankar and H. H. Hu. A numerical investigation of the detachment of the trailing particle from a chain sedimenting in Newtonian and viscoelastic fluids. J. Fluids. Engineering, **122**, 517-521 (2000)